American Journal of Nano Research and Applications
2019; 7(4): 27-38
http://www.sciencepublishinggroup.com/j/nano
doi: 10.11648/j.nano.20190704.11
ISSN: 2575-3754 (Print); ISSN: 2575-3738 (Online)

Review Article

On Guided Remagnetization in Layered Anoheterostructures

Andrii Korostil

Department of Magnetic Mesoscopic Materials and Nanocrystalline Structures, Institute of Magnetism, Kyiv, Ukraine

Email address:
korostilandrii@gmail.com

To cite this article:
Andrii Korostil. On Guided Remagnetization in Layered Anoheterostructures. *American Journal of Nano Research and Applications*. Vol. 7, No. 4, 2019, pp. 27-38. doi: 10.11648/j.nano.20190704.11

Received: November 28, 2019; **Accepted**: December 27, 2019; **Published**: January 31, 2020

Abstract: Field-guided magnetic dynamics in magnetic multilayer nanostructures involves interconnection of the control field with localized spin states, which can occur directly or indirectly depending on the nature of the field and spin polarization. At the control electromagnetic field, this interconnection can be directly induced by the photon-induced spin-flip processes and indirectly by a bias field during antiferromagnetic exchange relaxation. The control impact of electric field and electric current on the magnetic states occurs indirectly via the spin polarization and spin current in combination with the exchange interaction of these polarized spins with localized magnetic states. The corresponding description of the magnetic dynamics is based on the modified Landau-Lifshitz equation and spin diffusion equations, taking into account the spin Hall and the inverse spin Hall effects for systems with normal metal sublayers. In the case of the magnetic nanostructures with the Rashba spin-orbit interaction in interfaces, the electric field-controlled magnetization is realized via the Rashba field-induced spin polarization, and its exchange interaction with localized magnetic states. Corresponding description is based on a tight-binding model of spin-orbit-coupled electrons exchange coupled to the localized magnetic states.

Keywords: Magnetic Nanostructures, Laser-induced Remagnetization, Spin-orbit coupling, Spin Hall Effect, Rashba Spin-orbit Coupling, Electron Field-controlled Magnetization

1. Introduction

The external field-controlled magnetization of the multilayer magnetic nanostructures is based on the excitation of the coherent spin polarization, a spin current and their exchange interaction with localized magnetic states [1, 2]. The realization of such the control is determined by nature of the field, and the composition of the multilayer magnetic nanostructures [2]. In the case of the external electromagnetic (laser) field, the manipulation by the magnetization can be caused both by the effective internal bias field of the magneto-optic inverse Faraday effect (IFE) [1] and by the heating-induced effective internal bias field of the intersublattice exchange interaction during antiferromagnetic interaction relaxation [3-7].

The electric field-controlled magnetization can be related to the spin polarized current and the spin current generated from an entering electric current by the effective fields of the ferromagnetic exchange interaction and the spin Hall effect (SHE), respectively, coupled by the exchange interaction with the localized magnetic states. In these cases, the electric field-induced electric current is conversed to the spin polarized electric current under a magnetic polarizer or to the spin current under the spin-orbit interaction.

The electric field-controlled magnetization can occur directly via the Rashba spin-orbit interaction and its effective bias field causing the spin polarization of itinerant electrons in interfaces exchange coupled with the localized magnetic states [7, 8]. In this case, the external electric field can result in changes of a surface magnetic anisotropy, specifically, switching of the perpendicular magnetic anisotropy. In this case, the electric field-induced changes of the magnetic anisotropy are described in the framework of a tight-binding model of spin-orbit-coupled electrons which exchange-coupled to a background ferromagnetic order parameter.

For today, the problem of physical limits of the temporal and spatial scales of remagnetization is related to the pulsed

laser-induced magnetization. Using laser excitation with fs pulses made it possible to influence the magnetization on femtosecond timescales. The ultra-fast laser-induced demagnetization opens up possibilities to push further the limits of operation of magnetic devices. This ultra-fast process is characterized by a femtosecond demagnetization and a picosecond recovery [1].

The current-controlled magnetization realizing via the spin-polarized current is of considerable interest in the multilayer magnetic nanostructures with the tunnel barrier sublayers having the property of a spin polarization filter. Due to the spin-dependent scattering of the transmission current, with respect to the magnetic configuration in the magnetic nanostructure, and the mutual dependence of the magnetic configuration on the spin polarization, the tunnel magnetic nanostructures represent the applied interest for spintronic devices. These magnetic nanostructires with the tunnel barrier sublayers based on the magnesium oxide compounds are characterized by high magnetoresistive effect and are utilized as sensing elements in magnetoresistive elements, as non-volatile memory elements and as high-density magnetoresistive random-access-memory (MRAM) cells [2].

The current-controlled magnetization realized via the spin current, which is generated by the SHE in magnetic multilayer nanostructures with heavy metal sublayer, in contrast to the case of the spin-polarized current is not related to the charge transfer through interfaces**.** In this case, the spin current causes the torque on magnetic moments by direct transfer of spin angular momentum, enabling manipulation of nanoscale magnetic devices. It so doing, the incoming current density is orders of magnitude lower than using the spin-polarized current [8].

The electric field controlled magnetization and the magnetic anisotropy in the magnetic multilayer nanostructures with the interface Rashba spin-orbit interaction is characterized by ultralow power consumption. It is related to the voltage-induced symmetry change and the change in the relative occupation of electron orbitals of magnetic atoms adjacent to the barrier insulating sublayers [13−15].

In the present paper, it is proposed the self-consistent sequential description of the field-controlled magnetic dynamics in the multilayered magnetic nanostructures based on the conception of the effective internal bias field together with the exchange interaction with the localized magnetic states.

The paper is organized as follow. In Sec. 2, it is described the laser-controlled remagnetization as the combined effect of the pulsed laser-induced heat demagnetization followed by the effective internal magnetic biasing. The cases of the effective internal bias field related to the IFE and the relaxation of the AF exchange interaction are considered. Section 3 is devoted to the electric current-controlled magnetization via the spin-polarized current and the spin current caused by the ferromagnetic exchange interaction and the SHE, respectively. By solving the spin diffusion process in the presence of the SHE, it is described the dynamic feedback sustains a steady-state magnetization dynamics. Section 4 is devoted to the problem of the electric field-controlled magnetization and the magnetic anisotropy energy in the multilayer magnetic nanostructures with heavy metal sublayers. In the tight-binding model of spin-orbit-coupled electrons exchange-coupled to a background ferromagnetic order parameter it is described the dependence of the magnetic anisotropy on the electron structure of the system and an electron band filling.

2. Electromagnetic Field-driven Magnetization

The impact of pulsed electromagnetic (laser) radiation on localized magnetic states of magnetic nanostructures can be caused both by the magnetic bias field of spin-orbit interaction of spin-polarized electrons excited by circularly polarized photons [1] and the magnetic bias field of the antiferromagnetic (AF) exchange interaction relaxing after the pulsed heat demagnetization [1, 2, 7]. Both cases are characterized by ultrafast magnetic switching.

2.1. Magnetization Controlled by Pulse Circularly Polarized Radiation

Equation Chapter 1 Section 1A direct impact of the circularly polarized laser radiation on magnetic states of magnetic nanostructures represents a combined effect of electron-photon excitation and coherent spin-orbit-induced spin flips, known as the magneto-optic IFE. The corresponding effective internal magnetic field is described by the expression [1, 2],

$$\vec{H}_{\mathrm{IFE}} = \alpha\left[\vec{E}(\omega)\times\vec{E}(\omega)^{*}\right], \tag{1}$$

where α is the tensor of magneto-optical susceptibility, $\vec{E}(\omega)$ is the electric field, ω is the frequency.

Under the circularly polarized laser irradiation, photon-excited electron wave functions becomes a superposition of several eigenstates that effectively increase the electron orbital moment leading to an increased spin-orbit coupling and thus resulting in an intensification of the spin-flip process. The spin-flip in the ground state is because circularly polarized light mixes a fraction of excited-state wave function into the ground state and causes the perturbed ground state to have a net magnetic moment. Duration of the spin-flip process is defined by the energy of the spin-orbit interaction in the perturbed electron states. For a material with a large magneto-optical susceptibility the spin-orbit coupling may exceed 20 meV and thus spin flip process can be as fast as about 20 fs.

Formation of the effective magnetic field of the IFE occurs with a time delay relatively the laser-induced heat demagnetization. The temperature dependence of the magnetic ordering parameter is characterized by the longitudinal relaxation in addition to the transverse relaxation

characterizing the angle variation of the magnetic order vector.

The corresponding macroscopic motion equation can be considered as a generalization of the atomistic approach containing the modified stochastic Landau-Lifshitz equation [1, 2],

$$\frac{d\vec{s}}{dt} = \gamma\left[\vec{s}\times\left(\vec{H}_{ef}+\vec{\xi}\right)\right] - \gamma\lambda\left[\vec{s}\times\left[\vec{s}\times\left(\vec{H}_{ef}+\vec{\xi}\right)\right]\right], \quad (2)$$

where

$$\left\langle \chi_\alpha(t)\chi_\beta(t)\right\rangle = \left(2\lambda T/\gamma\mu_0\right)\delta\left(t,t'\right),$$

for the classical atomic spin moment $\boldsymbol{s}$, where λ is the parameter of the coupling to the bath system ($\lambda<0$, $|\lambda|>>1$), and second equation describes the correlation of the components of the Langevin field component, $\boldsymbol{\xi}(t)$ (T is the temperature). It is assumed, that the magnetic field $\vec{H}_{ef}$ contains the effective magnetic field of the IFE. Ensemble-averaging (2) results in the Landau-Lifshitz-Bloch (LLB) equation [5, 7]

$$\frac{d\vec{m}}{dt} = \gamma\left[\vec{m}\times\vec{H}_{ef}\right] - (\gamma\alpha_{\|}/m^2)\left(\vec{m}\cdot\vec{H}_{ef}\right)\vec{m}$$

$$+(\gamma\alpha_{\perp}/m^2)\left[\vec{m}\times\left[\vec{m}\times\vec{H}_{ef}\right]\right], \quad (3)$$

where $\vec{m}=\mu_0<\vec{s}>$, $\lambda_{\|}=\lambda(2T\Omega)$ and $\lambda_{\perp}=\lambda(1-\Omega)$ (here $\Omega=1/T^{MF}$) are the dimensionless longitudinal and transverse parameters, respectively, T^{MF} is the mean-field Curie temperature.

A complete description of magnetic dynamics includes the temporal evolution of the electron, spin and lattice temperatures, T_e, T_s and T_l, respectively. This temporal evolution is described in the three-temperature model by the system [1, 2],

$$C_i dT_i/dt = C_{ij}(T_i - T_j) + \delta_i P(t),\ i,j=(e,l,s), \quad (4)$$

where C_{ij} represents the coupling between the *i*th and *j*th baths, C_i is their heat capacity, and $P(t)$ is the laser-induced heat pulse, duration of which is defined by the laser pulse duration. Depending on the heat capacities C_i, effective temperature differences can be very large. Since the electron heat capacity is typically one to two orders of magnitude smaller than that of the lattice, T_e may reach several thousand Kelvin within the first tens of femtoseconds after the laser excitation, while the lattice remains relatively cold even after the equilibration processes.

In accordance with (3) and (4), the magnetization dynamics involves the primary heat demagnetization under the laser pulse and a subsequent biasing by the effective magnetic field of the IFE. Hence, formation of the bias field must begin after the heat-induced demagnetization as it is shown in Figure 1 [3, 4].

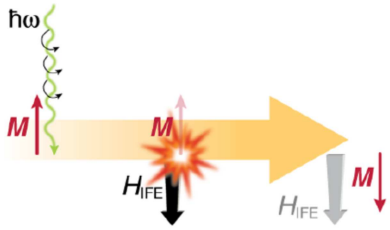

Figure 1. *The magnetization ($\vec{M}$) switching by a short and intense circularly polarized laser pulse. Shortly after the pulse, magnetization collapses due to heating. During the cooling, $\vec{M}$ restores along the effective field.*

The laser-induced remagnetization can only occur when the intensity and pulse duration of the circularly polarized laser radiation are related in a particular way [5, 6].

2.2. Heat Remagnetization Under by Pulse Linearly Polarized Radiation

Magnetic dynamics of two-sublattice ferrimagnetic compound (e. g., GdFeCo) under the impact of the laser-induced heat pulse is described by the modified Landau-Lifshitz-Bloch (LLB) equations [5, 6],

$$\frac{1}{|\gamma_\nu|}\frac{d\vec{m}_\nu}{dt} = -\vec{m}_\nu\times\left[\vec{\mathrm{H}}_{\nu'}^{EX} + \frac{\alpha_\nu^{\perp}}{m_\nu^2}\times\vec{\mathrm{H}}_\nu^{EX}\right] + \alpha_\nu^{\|}H_\nu^{Ex}\vec{m}_\nu, \quad (5)$$

where $\nu=(TE,RE)$, $\vec{m}_\nu$ is magnetization of element ν, *TE* and *RE* are the transition (Fe) and rare-earth (Gd) elements, respectively, γ_ν is the gyromagnetic ratio, $\alpha_\nu^{\|}$ and $\alpha_\nu^{\perp}$ are transverse and longitudinal damping parameters, $\mathbf{H}_\nu^{EX}$ is the exchange field from the ν th magnetic sublattice in a mean field approximation. RE is calculated via the mean-field approximation. The equation (5) together with (4) describes magnetic dynamics of the each sublattice and the total magnetic dynamics of the ferrimagnetic.

Solving (4) and (5) results in the "ferromagnetic-like" transitional magnetic state with subsequent remagnetization of the magnetic sublattices. For the ferrimagnetic GdFeCo compound this laser-induced remagnetization is demonstrated n Figure 2 [7].

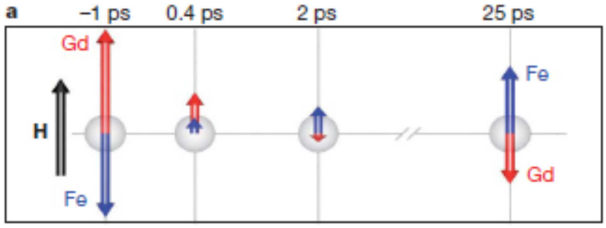

Figure 2. *The non-equilibrium dynamics of the Fe and Gd magnetizations with respect to an external magnetic field H.*

At the strong enough spin-orbit coupling the interaction of sublattice magnetizations with the lattice becomes dominant and remagnetization becomes impossible.

3. Electric Field and Spin-orbit-controlled Magnetization

The electric field-controlled magnetization of the magnetic nanostructures with strong enough spin-orbit interaction is related to the electron spin polarization which can be caused both by the SHE of converting an electric current to the transverse spin current [8] and by the effective field $\boldsymbol{B}_R$ of the Rashba spin-orbit interaction [9]. In the both case the impact on the localized magnetic state occurs via the exchange interaction. In the first case, the impact of the electric field is realized via the exchange coupling the localized magnetic states with the spin polarization and the spin current, in the second case.

3.1. Spin-polarized current-induced Torque on Magnetization

The electric field current manipulation by the localized magnetic states in multilayer nanostructures can be realized via a spin current and its exchange interaction with localized magnetization. The spin current can be generated both by the exchange magnetic interaction of the magnetic polarizer and by the SHE converting the charge current into transverse pure spin current without charge transfer.

The spin current interacts with localized magnetic moments via the exchange spin torque. The effect of the spin torque is modeled by an *s-d* exchange Hamiltonian, $H_{sd} = -J_{ex}\vec{s}\cdot\vec{S}$, where $\vec{s}$ and $\vec{S}$ are the spins of itinerant and localized electrons, respectively, and J_{ex} is the exchange coupling strength between them. In fact, the *s-d* model captures most of the physics on the interplay between spin-polarized transport and the magnetization dynamics of local magnetic moments.

The quantum-statistical averaged Schrödinger equation for the averaged local spin operator, $\vec{M} = \langle\vec{S}\rangle$ (here $\langle\cdots\rangle$ denotes averaging) with an added phenomenological damping terms is known as the Landau-Lifshitz-Gilbert-Slonczewski (LLGS) equation [1, 8],

$$\frac{\partial\vec{M}}{\partial t} = -\gamma\left[\vec{M}\times\vec{H}_{eff}\right] + \alpha\left[\vec{M}\times\frac{\partial\vec{M}}{\partial t}\right] - \gamma\frac{J_{ex}}{\mu_B}\left[\vec{m}\times\vec{M}\right], \quad (6)$$

describing magnetization dynamics under the spin current. The last term on the right hand side contains a spin density $\vec{m} = \langle\vec{s}\rangle$. Clearly, that only the transverse spin density $\vec{m}$ influences on the magnetization state via the spin torque [2],

$$\vec{T} = -\gamma\frac{J_{ex}}{\mu_B}\left[\vec{m}\times\vec{M}\right] = -\left(\alpha\left[\vec{M}\times\vec{P}\right] - \beta\left[\vec{M}\times\left[\vec{M}\times\vec{P}\right]\right]\right), \quad (7)$$

where $\alpha = \gamma J_{ex} m_x / \mu_B$ and $\beta = -\gamma J_{ex} m_y / \mu_B$ in the considered free-electron approximation, $\vec{P}$ is the initial vector of spin polarization before the interaction of the spin current with local magnetization. The first term on the right-hand-side of the equation (7) is so-called field-like term (out-of-plane torque) and the second term is the Slonzhevski term (or in-plane torque). At a certain threshold spin currents density level (which for the spin-polarized currents is of the order 10^8 A/cm^2) the spin torque can cause magnetization switching.

The equation of motion for the density magnetization has the form,

$$\frac{\partial\vec{m}}{\partial t} = -\nabla\vec{J}_s + \vec{T} + \vec{R}, \quad (8)$$

where $\vec{J}_s$ is the spin current density, $\vec{R} = 0$ in the ballistic case and $\vec{R} = \vec{m}/\tau_{sf}$ in the diffusion case (τ_{sf} is the spin-flip time). Due to the quasi-stationary dynamics of the magnetic density, the spatial transfer of spin density from spin current to localized spins is equivalents to the spin torque.

The current-induced spin torque near magnetic/nonmagnetic interfaces is formed via the spin-dependent scattering when the transverse component of spin quantum state of the incident spin flux is absorbed and the effective spin torque on the layer magnetic moment is generated.

3.2. Electric Current Spin-orbit Guided Magnetization

The electric current control of magnetization in the ferromagnet (FM)/normal heavy metal (N) nanostructures is closely related to the problem of sustaining the uniform steady-state magnetization dynamics. Solving this problem involves using the SHE of the spin-orbit-induced conversion of the electric current into the transverse spin current, and the inverse spin Hall effect (ISHE) of the conversion of the spin current into the transverse electric current [1, 2].

In such the magnetic nanostructures with the SHE the induced magnetic dynamics is accompanied by reciprocal processes of the spin torque and spin pumping, whose interplay leads to a dynamic feedback effect interconnecting energy dissipation channels of both the magnetization and electric current.

Characteristic properties of the electric current-induced magnetic dynamics in the presence of the SHE are exhibited in the model bilayer magnetic nanostructure, insulation ferromagnet (IF)/SHE normal metal (NM) with the effective magnetic field of the magnetization precession along the Cartesian axis x, the electric current applied along the axis y and the spin current along the axis z (Figure 3) [8].

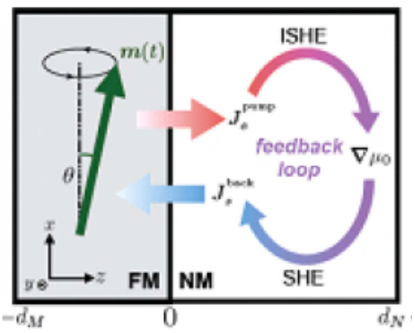

Figure 3. *The interconnection between the magnetization procession and the electric current $\vec{I}_c = \vec{\nabla}\mu_0$ (μ_0 is an electrochemical potential) via spin pumping, the ISHE, the SHE and spin backflow closed in the feedback loop.*

The closure of reciprocal processes of the spin torque and spin pumping via SHE and ISHE into the feedback loop is described by the system [8],

$$\begin{aligned}\frac{\partial\vec{\mu}}{\partial t} &= D\frac{\partial^2\vec{\mu}}{\partial z^2}-\frac{1}{\tau_{sf}}\vec{\mu},\\ \vec{J}_c &= -\frac{\sigma_r}{2e}\left[\vec{\nabla}\mu_0+\theta_s z\times\frac{\partial\vec{\mu}}{\partial z}\right],\\ \vec{J}_s &= -\frac{\sigma_r}{2e}\left[\frac{\partial\vec{\mu}}{\partial z}+\theta_s z\times\vec{\nabla}\mu_0\right],\end{aligned} \tag{9}$$

with the boundary condition,

$$\vec{J}_S(z)_{z=0} = \vec{J}_{s0} = (G_r/e)\left(\left[\vec{m}\times[\vec{m}\times\vec{\mu}_{s0}]\right]+\hbar[\vec{m}\times d\vec{m}/dt]\right). \tag{10}$$

The first equation in (9) describes the diffusion of the spin accumulation $\vec{\mu}$ (the non-equilibrium spin density of itinerant electrons in NM), the second and third equations describe the charge and spin current densities $\vec{J}_c$ and $\vec{J}_s$, respectively, at the spin Hall effect in the normal metal sublayer. In addition, $\mu_0/2$ is the electrochemical potential, D is the diffusion constant, σ_r is the conductivity, θ_S is the spin Hall angle and G_r is the real part of the spin-mixing conductance [8], in (10) the subscript zero means the value at the interface.

The first and second terms of the boundary condition (10) represent the spin torque and the spin pumping, respectively. Solving (9) and (10) results in the equation [8],

$$\begin{aligned}\frac{d\vec{m}}{dt} &= \gamma\vec{H}_{eff}\times\vec{m}+\omega_s\vec{m}\times\left[(z\times\vec{j}_c)\times\vec{m}\right]+(\alpha_0+\alpha_{sp})m\times\frac{d\vec{m}}{dt}\\ &+\alpha_{fb}\left(m_z^2\vec{m}\times\frac{\partial\vec{m}}{\partial t}+\frac{\partial m_z}{\partial t}\vec{m}\times\vec{z}\right),\end{aligned} \tag{11}$$

where $\vec{j}_c = \vec{J}_c/J_c$, and

$$\omega_s = \theta_s J_c\frac{\hbar\gamma}{eM_s d_M}\frac{\lambda G_r\tanh\frac{d_N}{2\lambda}}{\sigma_r+2\lambda G_r\coth\frac{d_N}{\lambda}}, \tag{12}$$

$$a_{sp(fb)} = \frac{(\lambda\theta_s^2\beta)^{0(1)}\hbar^2\gamma}{2e^2M_s d_M}\frac{\sigma G_r}{(\sigma_r+2\lambda G_r\beta)^{1(2)}} \tag{13}$$

($\beta=\coth(d_N/\lambda)$). Here ω_s is the strength of the spin torque, a_{sp} describes the conventional enhanced damping from the spin pumping with the spin backflow, the term a_{fb} reflects the dynamic feedback induced by the combination of the SHE and ISHE.

The feedback-induced damping is qualitatively described by two last equations in (9). Increase of the magnetization procession results in an increase of the pumped spin current $\vec{J}_{s0}$ and the spin diffusion $\partial_z\vec{\mu}$ according to the third relation. This leads to the larger electromotive force $\vec{\nabla}\mu_0$ in the NM according to the second relation at the fixed electric current, $\vec{J}_c$. The change of $\vec{\nabla}\mu_0$ will eventually feed back into $\vec{J}_s$ limiting its further growth. As consequence, the growing magnetization precession is inhibited.

4. Electric Field Rashba Spin-orbit-driven Magnetization

Bilayers containing an interface between a thin layers of a heavy-metal and a magnetic one are important hybrid materials in spintronics, as they combine magnetic order, strong spin-orbit interaction, and an broken inversion symmetry. This together with exchange interactions of the magnetic layer can lead to perpendicular magnetic anisotropy (PMA) [9], Dzyaloshinskii-Moriya interactions [10, 11] spin-orbit torques, Rashba-Edelstein effects, and more [12]. Spin-orbit interactions near the interface provide a handle to alter these properties by tuning chemical composition, interface structure, or gate voltages, as demonstrated most extensively for magnetic anisotropy [13, 14].

4.1. Controlled Magnetic Anisotropy in the Free-electron Model

Equation Chapter 1 Section 1 An electric field applied to the two-dimensional electron system of the interfaces via breaking an inverse symmetry and spin-splitting with spin polarization due to *s-d*-exchange interaction can form a perpendicular magnetic field changing the total surface magnetic anisotropy. The perpendicular surface magnetic anisotropy is formed in the bilayers composed of the magnetic sublayer based on 3d transition metals and heavy metal sublayer with the strong enough spin-orbit interaction.

The interface magnetization of the bilayer magnetic nanostructure is described in the free electron approximation by the Hamiltonian, containing the band Stoner model with the spin-orbit Rashba interaction [9],

$$H = \frac{p^2}{2m}-J_0\vec{S}\cdot\vec{\sigma}+\frac{\alpha_R}{\hbar}\left(\sigma_x p_y-\sigma_y p_x\right), \tag{14}$$

where $\vec{p}$ is the electron momentum operator, $\vec{S}$ is the order parameter, $\vec{\sigma}$ is the Pauli matrix vector, J_0 is the exchange interaction between itinerant electrons and localized magnetic moments, and $\alpha_R = e\eta_{so}E$ is the Rashba parameter proportional to η_{so} which describes spin-orbit coupling. It is assumed, that the electric field is pointed along the axis z ($\vec{E}=E\vec{z}$) and the unite vector $\vec{m}=\vec{S}/S$ is defined as $\vec{m}=(0,\sin\theta,\cos\theta)$ in the Cartesian coordinate system with the axis z perpendicular to the interface.

Solving spectral problem for the Hamiltonian (14) results in the θ dependent single particle energy [9],

$$\varepsilon_{k\sigma} = \frac{\hbar^2}{2m}\left[(k_x-\sigma k_0\sin^2\theta)^2+k_y^2\right]-E_R\sin^2\theta$$

$$-\sigma\left[(J_0S)^2+\alpha_R^2(k_x^2\cos^2\theta+k_y^2)\right]^{1/2}, \quad (15)$$

where

$$E_R = m\alpha_R^2/2\hbar^2 = -(m(e\eta_{SO})^2/2\hbar^2)E^2. \quad (16)$$

Here $\boldsymbol{k}=\boldsymbol{p}/\hbar$, $\sigma=\pm1$ is the spin quantum number, $k_0=ma_R/\hbar$ is the momentum shift, $\alpha_R \sim E$ is the Rashba parameter. The direction of the momentum shift in (15) changes sign as the spin index, $\sigma=\pm1$. These shifts also change sign with $\vec{m}\to -\vec{m}$ for a given σ, that reflects the Rashba spin splitting. E_R in (15a) reflects the single particle energy gain relatively to zero electric field ($E=0$).

At $(J_0S)^2 > (\alpha_R k_x)$ in the linear approximation in E^2 (15) after averaging over the Fermi sea takes the form,

$$E_{an} = E_R\left[1-\frac{2T}{J_0S}\right]\cos^2\theta,\ T=\frac{\hbar^2}{2m}\left(<k_x^2>_\uparrow - <k_x^2>_\downarrow\right), \quad (17)$$

where $\langle\cdots\rangle$ denotes an average over the Fermi sea. Thus, the Rashba spin-orbit interaction produces an perpendicular magnetic anisotropy of second order in the external electric field, E. The Rashba magnetic field due to the internal electric field in the surface region of an ultra-thin ferromagnet can make an important contribution to the perpendicular magnetic anisotropy.

4.2. Driven Magnetic Anisotropy in a Tight-binding Model

Magnetic anisotropy energy (MAE) refers to the dependence of the total energy of a magnetic system on the real-space orientation of its magnetization. The MAE is responsible for the orientational stability of magnetic domains, and hence lies at the heart of both magnetic hard disk drives and magnetic random access memories. There are two main contributions to the MAE: the magnetocrystalline anisotropy, which arises from electronic spin-orbit interactions, and shape anisotropy which arises from the magnetostatic dipolar interaction. For a thin ferromagnetic film, the magnetostatic energy is minimizedwhen the magnetization is in the plane of the film, leading to in-plane magnetic anisotropy (IMA).

To stabilize perpendicular magnetic anisotropy (PMA), the magnetocrystalline anisotropy energy must overcome the shape anisotropy. From the technological point of view, PMA is very important, since it enables an increased bit storage density, through a reduced size of the magnetic domains that store each bit of information. Solving this problem involves description of the magnetocrystalline anisotropy of a ferromagnet/heavy-metal bilayer, driven by interfacial Rashba SOC, highlighting different physical regimes [15]. The corresponding description is based on an electron tight-binding model, which allows to analyze the MAE with respect to the three competing energy scales: the non-relativistic kinetic energy t', the Rashba SOC strength t'', and the strength of the exchange coupling J to the ferromagnetic order parameter. This leads to conditions for the realization of the PMA and its dependence on the electron structure.

4.2.1. Model of Two-layer Magnetic Nanostructure with a Rashba Effect

The properties of itinerant electrons with broken inversion symmetry and SOC in a two-dimensional lattice with one orbital per site, nearest-neighbor hopping, and Rashba-like spin-momentum is described by the Hamiltonian [15]

$$H_e = -\frac{1}{2}\sum_{<i,j>}\sum_{s,s'} c_{is}^{?}\left(t'\sigma_{ss'} - it''\left[\vec{z}\times\vec{R}_{ij}\right]\cdot\vec{\sigma}_{ss'}\right)c_{js'}. \quad (18)$$

Here the sum is over near-neighbor links, $c_{is}^{\dagger}$ and c_{js} arethe creation and annihilation operators for an electron with spin s at a lattice site $\vec{R}_i$, $\sigma_{ss'}^0$ is the unit 2×2 spin matrix, and $\sigma=(\sigma^x,\sigma^y,\sigma^z)$ is the vector of Pauli matrices. The vector connecting site i to site j is $\vec{R}_{ij}=\vec{R}_i-\vec{R}_j$, and the cross product favors spin-orientations perpendicular to the bond direction, $\hat{R}_{ij}=\vec{R}_{ij}/|\vec{R}_{ij}|$ and the normal to the lattice plane, z. The hopping strength is given t, and the angle ϕ_R characterizes the relative strength of conventional spin-independent hopping, $t'=2t\cos\phi_R$ and chiral Rashba hopping $t''=2t\sin\phi_R$. It is imposed Born-von Karman periodic boundary conditions and introduced the lattice Fourier transforms of the operators, $c_{is}=\sum_{\vec{k}} e^{i\vec{k}\vec{R}_i}$, where N is the number of lattice sites and $\vec{k}$ is the electron pulse.

This transforms the Hamiltonian (17) to the form,

$$H_e(\vec{k}) = H_0(\vec{k}) + H_R(\vec{k}), \quad (19)$$

where

$$\begin{aligned} H_0(\vec{k}) &= -t'\left(\cos k_x+\cos k_y\right)\sigma^0,\\ H_R(\vec{k}) &= -t''\left(\sin k_x\sigma^y - \sin k_y\sigma^x\right). \end{aligned} \quad (20)$$

For small k, the Hamiltonian (19) describes a Rashba electron gas

The total Hamiltonian also involves the ferromagnetic interaction between quasiparticles and magnetic condensate, $H_B=-\vec{B}\cdot\vec{\sigma}$, i.e.,

$$H(\vec{k}) = H_e(\vec{k}) + H_B = E_0(\vec{k})\sigma^0 + \vec{b}(\vec{k})\cdot\vec{\sigma}, \quad (21)$$

where

$$\begin{aligned} E_0(\vec{k}) &= -t'\left(\cos k_x+\cos k_y\right),\\ \vec{b}(\vec{k}) &= \vec{b}_R(\vec{k})+\vec{B},\\ \vec{b}_R(k) &= t''\left(\sin k_y\vec{x}\text{-}\sin k_x\vec{y}\right),\\ \vec{B} &= J\left(\sin\theta\left(\cos\varphi\vec{x}+\sin\varphi\vec{y}\right)\right)+\cos\theta\vec{z}. \end{aligned} \quad (22)$$

Here $\vec{b}_R(\vec{k})$ is the Rashba spin-orbit field, and the coupling to the ferromagnetic background is given by $\vec{B}$, where the spherical angles θ and φ specify the magnetization orientation and J is the strength of the coupling.

In the diagonalized form the Hamiltonian,

$$H(\vec{k}) = E_+(\vec{k})P_+(\vec{k}) + E_-(\vec{k})P_-(\vec{k}), \quad (23)$$

where the band energies

$$E_\pm = E_0(\vec{k}) \mp |\vec{b}(\vec{k})| \quad (24)$$

and the eigenvector projectors

$$P_\pm(\vec{k}) = \frac{1}{2}\left(\sigma^0 \pm \hat{b}(\vec{k})\cdot\vec{\sigma}\right), \quad b(k) = \frac{\vec{b}(\vec{k})}{|\vec{b}(\vec{k})|}. \quad (25)$$

The plus sign corresponds to the lower energy majority band and the minus sign to the higher energy minority band. Band dispersions are plotted in Figure 1 for some representative cases.

The electronic density of states (DOS) is given by

$$\rho(E) = \sum_{n=\pm}\int \frac{d\vec{k}}{(2\pi)^2}\delta\left(E - E_n(\vec{k})\right), \quad (26)$$

which leads to the number of electrons per lattice site,

$$N(E) = \int \frac{d\vec{k}}{(2\pi)^2}\delta\left(f_+(\vec{k}) - f_+(\vec{k})\right) = \int_{-\infty}^{E_F} dE\rho(E). \quad (27)$$

The integral in (27) is over the first Brillouin zone, and the function, $f_n(\boldsymbol{k}) = \theta\left(E_F - E_n(\boldsymbol{k})\right)$ describes the occupation of the corresponding eigenstate, $E_n(\boldsymbol{k})$. The coupling to the ferromagnetic background induces a net spin moment on the itinerant electrons, given by

$$\vec{M} = \int \frac{d\vec{k}}{(2\pi)^2}\left(f_+(\vec{k}) - f_-(\vec{k})\right)\hat{b}(\vec{k}) = \int_{\infty}^{E_F} dE\,\vec{m}(E), \quad (28)$$

where $\vec{m}(E)$ is the spin-polarized density of electron states (DOS). The energetics of the itinerant electrons can be obtained from the internal energy, which at zero temperature is defined as

$$U = \sum_{n=\pm}\int \frac{d\vec{k}}{(2\pi)^2} f_n(\vec{k})E_n(\vec{k}) = \int_{-\infty}^{E_F} dE\rho(E)E, \quad (29)$$

Due to additivity contributions of the bare band, Rashba, and exchange interactions to the internal energy,

$$U = \sum_{n=\pm}\int \frac{d\vec{k}}{(2\pi)^2} f_n(\vec{k})\,\mathrm{Tr}\,P_n(\vec{k})H(\vec{k}) = U_0 + U_R + U_B. \quad (30)$$

Solving the Hamiltonian (19) is based on the Green function,

$$G(\vec{k}, E) = \left(E - H(\vec{k})\right)^{-1} = \sum_{n=\pm}\frac{P_n(\vec{k})}{E - E_n(\vec{k})}, \quad (31)$$

which, specifically, is related to the internal energy and its derivatives. For instance, the DOS and the spin-polarized DOS are given by

$$\rho(E) = -\frac{1}{\pi}\mathrm{Im}\mathrm{Tr}\int \frac{d\vec{k}}{(2\pi)^2}G(\vec{k},E) \quad (32)$$

and

$$\vec{m}(E) = -\frac{1}{\pi}\mathrm{Im}\mathrm{Tr}\int \frac{d\vec{k}}{(2\pi)^2}\sigma G(\vec{k},E), \quad (33)$$

respectively, where the traces are over the spin components. The uniform static spin susceptibility for a fixed number of electrons is determined as

$$\chi^{\alpha\beta} = \frac{\partial M_\alpha}{\partial B_\beta} = -\frac{1}{\pi}\mathrm{Im}\mathrm{Tr}\int_{-\infty}^{E_F} dE\int \frac{d\vec{k}}{(2\pi)^2}\sigma^\alpha G(\vec{k},E)\sigma^\beta G(\vec{k},E) - R_{\alpha\beta}, \quad (34)$$

where $R_{\alpha\beta} = m^\alpha(E_F)m^\beta(E_F)/\rho(E_F)$ comes from ensuring that $\partial N_e/\partial B^\beta = 0$. Substitution the spectral representation of the Green function (31) into (34) results in the expression,

$$\chi^{\alpha\beta} = -\frac{1}{\pi}\mathrm{Im}\mathrm{Tr}\int \frac{d\vec{k}}{(2\pi)^2}\sum_{nn'}\int_{-\infty}^{E_F} dE\frac{\sigma^\alpha P_{n'}(\vec{k})}{E - E_{n'}(\vec{k})}\frac{\sigma^\beta P_n(\vec{k})}{E - E_n(\vec{k})} - R_{\alpha\beta}, \quad (35)$$

where summation over $n = n'$ corresponds to intraband electron transitions and, consequently, to the intraband part ($\chi^{\alpha\beta}_{\mathrm{intra}}$) of the magnetic susceptibility. Summation over $n \neq n'$ corresponds to interband electron transition and, consequently, to the interband part ($\chi^{\alpha\beta}_{\mathrm{inter}}$) of the magnetic susceptibility. Therefore, the total magnetic susceptibility is sum, $\chi^{\alpha\beta} = \chi^{\alpha\beta}_{\mathrm{intra}} + \chi^{\alpha\beta}_{\mathrm{inter}}$. The interband magnetic susceptibility, $\chi^{\alpha\beta}_{\mathrm{inter}}$, contains the integrand, the partial fraction decompositions of which, according to the Sokhotsky formula, leads to the relation,

$$-\frac{1}{\pi}\mathrm{Im}\mathrm{Tr}\int_{-\infty}^{E_F} dE\frac{1}{(E - E_n(\vec{k}))} = f_n(\vec{k}), \quad (36)$$

The intraband magnetic susceptibility, $\chi^{\alpha\beta}_{\mathrm{intra}}$, contains the integrand which is the partial fraction with a second order pole that results in the relation,

$$-\frac{1}{\pi}\mathrm{Im}\mathrm{Tr}\int_{-\infty}^{E_F} dE\frac{1}{(E - E_n(\vec{k}))^2} = \frac{\partial f_n(\vec{k})}{\partial E_n(\vec{k})}, \quad (37)$$

which is the partial derivative of (36) with respect to $E_n(\vec{k})$.

Taking into account (36) and (37) the intra- and interband magnetization susceptibilities can be represented as

$$\chi_{\text{intra}}^{\alpha\beta} = \int \frac{d\vec{k}}{(2\pi)^2} \overline{b_\alpha}(\vec{k}) b_\beta(\vec{k}) \sum_{n=\pm} \delta(E_F - E_n(\vec{k})) - R_{\alpha\beta} \qquad (38)$$

and

$$\chi_{\text{inter}}^{\alpha\beta} = \int \frac{d\vec{k}}{(2\pi)^2} \left(\overline{b_\alpha}(\vec{k}) b_\beta(\vec{k}) - \delta_{\alpha\beta} \right) \frac{f_-(\vec{k}) - f_+(\vec{k})}{E_-(\vec{k}) - E_+(\vec{k})}, \qquad (39)$$

respectively. The intraband term collects the contributions from the Fermi surface, while the interband term collects those from the Fermi sea.

Band dispersions given by (24) and respective densities of states essentially depend on the parameters t'' and J of the Rashba spin-orbit coupling strength and the exchange coupling to the ferromagnetic order parameter, respectively, as it is represented in Figure 4 [15].

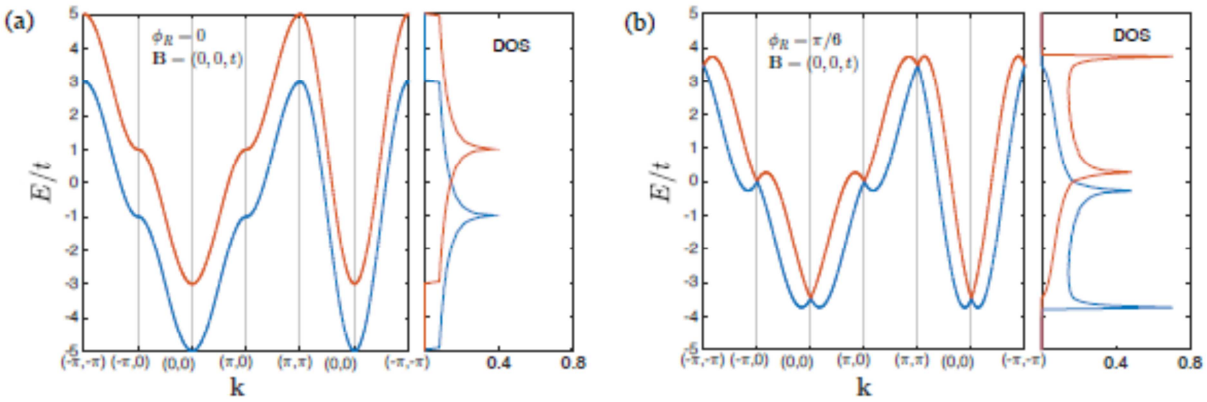

Figure 4. *Band and dispersions and the respective densities of states for representative cases: (a)* $\phi_R = 0$ $(t' = 2t, t'' = 0, J = t)$, *(b)* $\phi_R = \pi/6$ $(t' = \sqrt{3}t, t'' = t)$.

No the interfacial Rashba SOC ($t'' = 0$) and finite exchange coupling (J) to the background magnetization leads to a constant vertical splitting of the bands (Figure 4a). Finite Rashba SOC ($t'' \neq 0$) and no background magnetization ($J = 0$) leads to $\boldsymbol{k}$ -dependent horizontal splitting of the bands (Figure 4b). The finite Rashba SOC and background magnetization lead to dependence of the dispersion on the orientation of the magnetization with respect to the lattice. When the magnetization is normal to the plane ($\boldsymbol{B} \parallel z$) the system has fourfold rotational symmetry. When the magnetization is along a nearest-neighbor direction ($\boldsymbol{B} \parallel x$) the bands have a unidirectional shift in the perpendicular direction (y).

4.2.2. Magnetic Anisotropy Energy

The MAE is due to the variation of the internal energy of the itinerant electrons as the ferromagnetic background orientation rotates. The MAE vanishes if there is no spin-orbit coupling, i.e. in the given model if there is no Rashba coupling ($\phi_R = t'' = 0$). Phenomenologically, the MAE is expanded in angular functions that respect the symmetry of the system [15]. For the square lattice (effectively tetragonal symmetry),

$$U_{MAE}(\theta, \varphi) \approx K_2 \sin^2\theta + (K_4 + K_4' \cos 4\varphi) \sin^4\theta \qquad (40)$$

with θ and φ the spherical angles describing the orientation of the ferromagnetic background. It follows from perturbation theory arguments that $K_{2n} \propto t''(t''/J)^{2n-1}$. Higher-order anisotropy constants should decline rapidly in magnitude, as they are proportional to higher powers of the ratio between the spin-orbit interaction strength and the spin splitting, which is often small. The anisotropy constants can then be determined by fitting the angular dependence of the internal energy. Keeping all other parameters fixed, the internal energy given by (30) is an explicit function of the angles describing the ferromagnetic orientation, $U(\theta, \varphi)$. Assuming that the model form in (40) holds, evaluating the internal energy for three orientations is sufficient to fix the anisotropy. The system will have PMA provided that both of the following inequalities are satisfied:

$$\left.\begin{aligned} U(\pi/2, 0) - U(0,0) &= K_2 + K_4 + K_4', \\ U(\pi/2, \pi/4) - U(0,0) &= K_2 + K_4 - K_4'. \end{aligned}\right\} > 0 . \qquad (41)$$

Here the magnetic anisotropy coefficients K_i as functions of the macroscopic parameters are determined by derivatives of the relation, $U = U_{MAE}$, with respect to the spherical angles, θ and φ . It can be shown that the anisotropy energy goes from IMA $\rightarrow$ PMA $\rightarrow$ IMA as function of the band filling.

The first and second derivative of the internal energy with respect to the ferromagnetic moment orientation are described by the expressions,

$$\begin{aligned} \frac{\partial U}{\partial \theta} &= \vec{M} \cdot \frac{\partial \vec{B}}{\partial \theta} = \left(K_2 + 2\left(K_4 + K_4' \cos 4\varphi \right) \sin^2\theta \right) \sin 2\theta, \\ \frac{\partial U}{\partial \varphi} &= -\vec{M} \cdot \frac{\partial \vec{B}}{\partial \varphi} = -K_4' \sin 4\varphi \sin^4\theta, \end{aligned} \qquad (42)$$

where $\boldsymbol{M}$ is the spin magnetic moment of the electrons defined in (28), and $\boldsymbol{B}$ is the effective magnetic field produced by the local moments defined in (22). From the phenomenological expression for $U_{MAE}(\theta, \varphi)$ it follows that the magnetic torque $[\vec{M} \times \vec{B}]$ vanishes for the high-symmetry nearest- and next-nearest-neighbor directions ($\theta = \pi/2$,

$\varphi = n\pi/4$) with $n = \{0,1,...,7\}$, and for magnetization normal to the lattice plane ($\theta = 0,\pi$). The second derivatives of the internal energy are particularly simple to evaluate for these high-symmetry directions, since cross derivatives involving both polar and azimuthal angles vanish. Therefore, it is required only the Cartesian component of the spin susceptibility tensor for the plane perpendicular to a chosen magnetization direction (i.e. only the transverse spin susceptibility are needed). For the high symmetry directions the net spin moment of the itinerant electrons is aligned with the ferromagnetic background, $\vec{M} \parallel \vec{B}$. For the in-plane high symmetry directions,

$$\begin{aligned} \frac{1}{2}\frac{\partial^2 U}{\partial \theta^2}\bigg|_{\vec{M}\parallel\vec{x}} &= \frac{J^2}{2}\left(\frac{M}{J} - \chi^{zz}\right) = -K_2 + 2\left(K_4 + K_4'\right), \\ \frac{1}{2}\frac{\partial^2 U}{\partial \varphi^2}\bigg|_{\vec{M}\parallel\vec{x}} &= \frac{J^2}{2}\left(\frac{M}{J} - \chi^{yy}\right) = -8K_4', \end{aligned} \tag{43}$$

and for the polar magnetization orientation,

$$\frac{1}{2}\frac{\partial^2 U}{\partial \varphi^2}\bigg|_{\vec{M}\parallel\vec{z}} = \frac{J^2}{2}\left(\frac{M}{J} - \chi^{zz}\right) = K_2 . \tag{44}$$

These equations determine the magnetic anisotropy constants via transverse components of the magnetic anisotropy susceptibility depending on the symmetry of the system. Consequently, the type of magnetic anisotropy (PMA or IMA) related to symmetry of the system. is determined MAE which dependence on the symmetry of the system. When $\vec{M} \parallel \vec{z}$, the system has fourfold rotational symmetry from which it follows that $\chi^{xx} = \chi^{yy}$ and $\chi^{xy} = \chi^{yx} = 0$.

Equations (43) and (44) contain a common term,

$$\bar{\chi} = \int \frac{d\vec{k}}{(2\pi)^2} \frac{f_+(\vec{k}) - f_-(\vec{k})}{|\vec{b}(\vec{k})|}, \tag{45}$$

whose subtraction gives the relation,

$$\chi^0 = \frac{M}{J} = \int \frac{d\vec{k}}{(2\pi)^2} \frac{\vec{B}\cdot\vec{b}_R(\vec{k})}{J^2} \frac{f_-(\vec{k}) - f_+(\vec{k})}{|\vec{b}_R(\vec{k})|}, \tag{46}$$

describing the volume susceptibility.

The expression for the intraband part of the spin susceptibility follows from (38) and does not contain $\bar{\chi}$:

$$\chi^{\alpha\alpha}_{\text{intra}} = \int \frac{d\vec{k}}{(2\pi)^2} (\hat{b}(\vec{k}))^2 \sum_{n=\pm} \delta(E_F - E_n(\vec{k})) . \tag{47}$$

Subtracting this term from the interband part of the spin susceptibility in (39) results in the equation,

$$\bar{\chi}^{\alpha\alpha}_{\text{inter}} = \chi^{\alpha\alpha}_{\text{inter}} - \bar{\chi} = -\int \frac{d\vec{k}}{(2\pi)^2} (\hat{b}_\alpha(\vec{k}))^2 \frac{f_+(\vec{k}) - f_-(\vec{k})}{|\vec{b}(\vec{k})|} . \tag{48}$$

In (47) and (48) $\alpha = x, y, z$, and $\hat{b}_\alpha(\vec{k})$ is the Cartesian component of the unit vector defining the spin quantization axis for each $\vec{k}$. As it is seen, $\chi^{\alpha\alpha}_{\text{intra}}$ is positive definite, while $\bar{\chi}^{\alpha\alpha}_{\text{inter}}$ is negative definite.

The magnetic anisotropy type, i.e. PMA or IMA, can be established in two ways. When $\boldsymbol{M} \parallel \boldsymbol{x}$ the longitudinal component, $\chi^{zz} = 0$, and the sign of the MAE is determined by χ^0. On the other hand, for $\vec{M} \parallel \vec{z}$ the volume susceptibility, $\chi^0 = 0$, so the sign of the MAE is decided by the competition between the intraband and interband contributions to the spin susceptibility χ^{xx}.

Conditions favoring PMA are determined by the magnetic anisotropy constants. When $\vec{M} \parallel \vec{z}$ and $t'' << J$, from (46) follows that,

$$\chi^{xx}_{\text{intra}} \approx \left\langle (\hat{b}(\vec{k}))^2 \right\rangle \int \frac{d\vec{k}}{(2\pi)^2} \sum_{n=\pm} \delta(E_F - E_n(\vec{k})) = \frac{(t'')^2}{2J^2} \rho(E_F) , \tag{49}$$

where $\rho(E_F)$ is the total density of states at the Fermi energy. The average of the matrix element was simplified by assuming that the exchange fields are much stronger than the spin-orbit fields, so that $|\vec{b}(\vec{k})| \approx -M(t'')^2/2J^3$. Combining these expressions leads to an approximate form, $K_2 \approx (M - J\rho(E_F))$ for the uniaxial anisotropy constant. The scale of anisotropy constant, $K_{\text{ref}} = (t'')^2/J$ is a useful figure of merit for MAE. PMA is likely to be stable when the density-of-states at the Fermi level is small: since $0 \le M \le 1$, it can expect PMA if $J\rho(E_F) \le 1$. The states at the Fermi level are the ones affected by SOC in the most important way, in energetic terms. A large DOS at the Fermi level then translates to a large number of single-particle states that gain the most energy from SOC once the magnetization is tilted away from the perpendicular direction, which explains why this contribution favors IMA.

4.2.3. PMA for the Gapped Half-filled Band Spectrum

In the case, in which the ferromagnetic exchange splitting is large enough to produce a gape for the half-filled ferromagnetic insulator, the Fermi level lies in this gape. The majority band is full, $f_+(\vec{k}) = 1$, and the minority band is empty, $f_-(\boldsymbol{k}) = 0$. Starting from (22), (24) and (29), the internal energy for this case is simply

$$U = \int \frac{d\vec{k}}{(2\pi)^2} \left(E_0(\vec{k}) - |\vec{b}(\vec{k})|\right), \tag{50}$$

where only the second term in the integrand contains information about the orientation of the ferromagnetic background, given by the angles θ and φ.

The expansion of the spin splitting $|\boldsymbol{b}(\boldsymbol{k})|$ gives its explicit dependence on the θ and φ, which have the form,

$$|\vec{b}(\vec{k})| = b_0(\vec{k}) \sum_{n=0}^{\infty} \binom{1/2}{n} \left(\cos\gamma(\vec{k})\right)^n , \tag{51}$$

where

$$b_0(\vec{k}) = \sqrt{|\vec{b}_R(\vec{k})|^2 + J^2},\ \cos\gamma(\vec{k}) = \frac{2\vec{B}\cdot\vec{b}_R(\vec{k})}{|\vec{b}_R(\vec{k})|^2 + J^2}.$$

The expansion (51) can be written more explicitly in the form,

$$|\vec{b}(\vec{k})| = \sum_{n=0}^{\infty}\sum_{p=0}^{n} B_n^p(\vec{k})(\sin\theta)^n\left(\cos\varphi\right)^p(\sin\theta)^{n-p} \quad (52)$$

with expansion coefficients,

$$B_n^p(\vec{k}) = (-1)^p 2^n\binom{1/2}{n}\binom{n}{p}\frac{(Jt'')^n(\sin k_y)^p(\sin k_x)^{n-p}}{\left(|\vec{b}_R(\vec{k})|^2 + J^2\right)^{n-1/2}}. \quad (53)$$

The internal energy then has the corresponding expansion,

$$U(\theta,\varphi) = \sum_{n=0}^{\infty}\sum_{p=0}^{n} U_n^p(\sin\theta)^n\left(\cos\varphi\right)^p(\sin\varphi)^{n-p} \quad (54)$$

with coefficients,

$$U_n^p = -\int\frac{d\vec{k}}{(2\pi)^2}B_n^p(\vec{k}) \quad (55)$$

Because the integrand is odd under $k_x \to -k_x$ and $k_y \to -k_y$, coefficients $U_n^{2p+1} = 0$ and $U_{2p+1}^k = 0$, i.e. only terms even in both p and n survive. In combination with the symmetry of the binomial coefficients, this also leads to the equality, $U_{2n}^{2n-2p} = U_{2n}^{2p}$.

Then, the first terms in the expansion are

$$U(\theta,\varphi) \approx U_0^0 + U_2^0\sin^2\theta + \frac{1}{8}\left(U_4^0 + U_4^2 + \left(2U_4^0 - U_4^2\right)\cos 4\varphi\right)\sin^4\varphi \quad (56)$$

in according with the phenomenological form given in (40).

For the gapped half-filled case, it is consistent to expand the integrand in the $|t''| << J$ limit,

$$B_0^0(\vec{k}) \approx J + \frac{|\vec{b}_R(\vec{k})|^2}{2J}\left(1 - \frac{|\vec{b}_R(\vec{k})|^2}{4J^3}\right),$$
$$B_2^0(\vec{k}) \approx -\frac{(t'')^2}{2J}\sin^2 k_x\left(1 - \frac{3|\vec{b}_R(\vec{k})|^2}{4J^2}\right), \quad (57)$$
$$B_4^0(\vec{k}) \approx -\frac{(t'')^4}{8J^3}\sin^4 k_x,\ B_4^2(\vec{k}) \approx -\frac{(t'')^4}{4J^3}\sin^2 k_x\sin^2 k_y$$

Substitution (57) into (55) results in the expressions,

$$U_2^0 = \frac{1}{4}\frac{(t'')^2}{J} - \frac{15}{64}\frac{(t'')^4}{J^3},\ U_4^0 = -\frac{15}{64}\frac{(t'')^4}{J^3},\ U_4^2 = \frac{1}{4}U_4^0, \quad (58)$$

describing the coefficients in the expansion of the internal energy (54).

Then, comparison (54) with the phenomenological expression (40) leads to the equations,

$$K_2 = \frac{1}{4}\frac{(t'')^2}{J} - \Delta,\ K_4 = -\frac{5}{8}\Delta,\ K_4' = -\frac{K_4}{5} \quad (59)$$

for the magnetic anisotropy coefficients. These anisotropy coefficients satisfy the PMA condition (39).

Thus, PMA is realized in the two-layered magnetic nanostructure composing of an insulating magnetic layer and heavy metal with the Rashba spin splitting effect in the case of the half-filled bands. In so doing, MAE depends directly on the exchange interaction between the spin-polarized iterant electrons and magnetic states of the ferromagnetic layer.

4.2.4. Physical Regimes of the MAE Forming

The magnetic anisotropy formation in the two-layered magnetic nanostructure, ferromagnetic/heavy metal, depends on the relations between parameters of the exchange interaction (J), kinetic energy (t') and the Rashba SOC (t''). Different interfacial magnetic states are determined by conditions of strong exchange ($J >> t' >> t''$), intermediate exchange ($J \sim t' >> t''$) and weak exchange ($t' >> J \sim t''$). It is assumed, that the SOC strength is smaller than the non-relativistic bandwidth. These three cases are defined by how the exchange energy due to the ferromagnetic coupling compares to these two energy scales. The magnetic anisotropy is determined by comparison of the local characterization of the MAE via the susceptibility with the global characterization via internal energy differences. For the present model, the contribution to the MAE from the volume susceptibility (46) vanishes when $\boldsymbol{M} \parallel z$, while it is the only non-vanishing contribution for $\boldsymbol{M} \parallel \boldsymbol{x}$.

In the first case, the domination of the exchange energy leads to two well separated bands. The dependence of the MAE on the number of electrons per lattice site (N_e), obtaining from the spin susceptibility, for two stable orientations of the ferromagnetic background, is characterized by PMA only in narrow range around $N_e = 1$ and by IMA for most values of N_e (Figure 5a).

When $\boldsymbol{M} \parallel z$ (44), the interband contribution to the susceptibility (48) favors PMA, while the intraband contribution (47) favors IMA. The amplitude of the intraband contribution is larger than the interband one, and is maximized when the Fermi level is at the Van-Hove singularity in the DOS of each band. When $N_e = 1$ and $\boldsymbol{M} \parallel z$, the intraband contribution must vanish because the system is gapped. Only the interband term remains finite and it favors PMA. When $\boldsymbol{M} \parallel \boldsymbol{x}$ (43), the volume susceptibility (46) is the only non-zero contribution, and reproduces essentially the same MAE as found for $\boldsymbol{M} \parallel z$. This agreement shows that the higher-order anisotropy constants (K_4 and K_4') are very small when compared with K_2. The MAE from the band energy difference between $\boldsymbol{M} \parallel \boldsymbol{x}$ and $\boldsymbol{M} \parallel z$ is in perfect agreement with the one extracted from the susceptibility (Figure 5b). The PMA is realized near half-filling. Moving from electron per site $N_e = 1$ to $N_e = 0$, the interband

contribution is accurately proportional to M, which decreases monotonically to zero. The intraband contribution qualitatively follows $\rho(E_F)$, which increases up to the Van-Hove singularity and then decreases again.

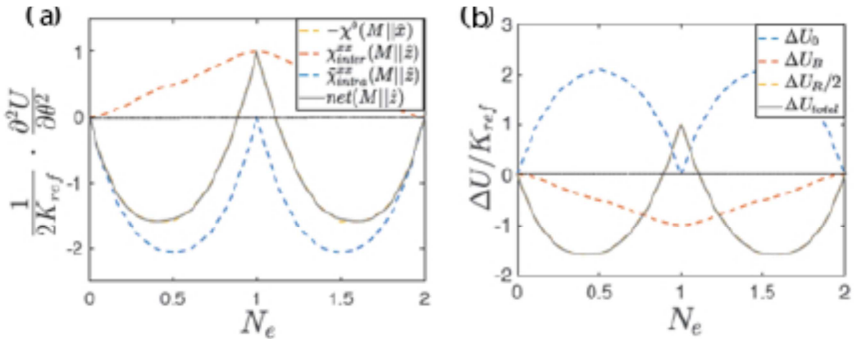

Figure 5. *MAE as the function of N_e for the strong exchange case, $J >> t' >> t''$. (a) The MAE from the second derivatives of the band energy, from the connection to its phenomenological form. (b) Internal energy differences decomposed using (30).*

In the second case, where the exchange energy is comparable to the non-relativistic band width by setting $J = t'$, the two bands overlap with minority band occupation beginning for $N_e > 0.5$, and the lower band being completely full for $N_e > 1.5$. This intermediate exchange coupling strength case is applicable to many ferromagnetic metals. The MAE from the spin susceptibility is characterized by PMA in a much wider range of N_e than in the strong exchange interaction case (Figure 6a).

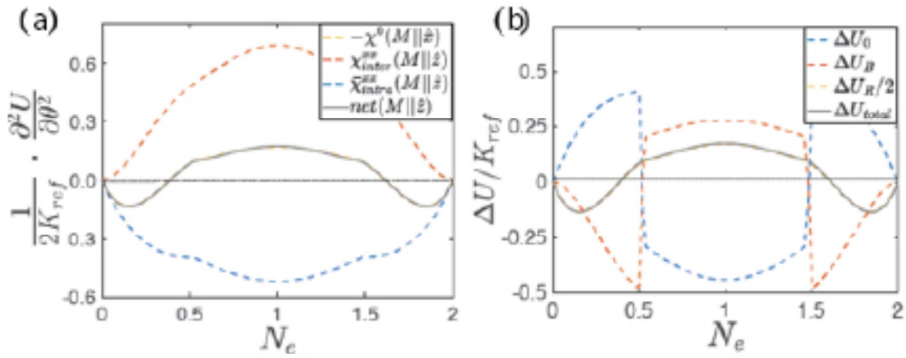

Figure 6. *MAE as the function of N_e for the strong exchange case, $J >> t' >> t''$. (b) The MAE from the second derivatives of the band energy, from the connection to its phenomenological form. (c) Internal energy differences decomposed using (30).*

Comparing (47) and (48), it appears that the Fermi sea term can be enhanced by reducing the k-dependent spin splitting, $|\boldsymbol{b}(\boldsymbol{k})|$, which follows from weakening J, so that the interband contribution has a larger amplitude than the intraband one. However, near $N_e = 0$ (likewise near $N_e - 2$), the intraband contribution is linear in N_e while the interband one is quadratic, so that the former can overtake the latter, and thus favors IMA. The MAE from the band energy difference between $\vec{M} \parallel \vec{x}$ and $\boldsymbol{M} \parallel z$ and its decomposition (Figure 6b) exhibits half of the difference in the SOC energy overlaps with the net internal energy difference. The energetic competition between the Rashba SOC and the coupling to the ferromagnetic background is settled differently when either only one or when both bands are partially filled, due to an allowed transfer of electronic occupation between the two bands at the Fermi sea.

In the third case where the exchange energy is comparable the SOC strength ($J = t''$) the splitting between the two bands is small. The intraband and interband contributions to the susceptibility are almost identical leading to a small net value of the MAE.

5. Conclusions

The pulse field manipulation by magnetic properties of multilayer magnetic nanostructures is based on an excitation of the coherent electron spin polarization coupled by the exchange interaction with localized magnetic states and heat-induced demagnetization. The impact of the pulse laser field on magnetic states can occur directly via the effective bias field of the inverse Faraday magneto-optic effect or indirectly via the laser-induced heat demagnetization with subsequent action of the effective bias field. The controlled impact of the strong enough laser field on the magnetic nanostructures with an antiferromagnetic exchange interaction occur due to the effective bias fields caused by the different time of the heat demagnetization of magnetic sublattices and the relaxation of the antiferromagnetic exchange interaction.

The electric field control can occur via the spin polarization of an electric current under the ferromagnetic exchange interaction in ferromagnetic layers and its exchange interaction with the localized magnetic states. In

multilayer magnetic nanostructures with the spin Hall effect the electric field control occur via a spin-orbit induced conversion of the electric current to the spin current coupled with the localized magnetic states by the exchange interaction.

The pure electric field can control the magnetic anisotropy in the magnetic nanostructures, with the Rashba spin-orbit interaction, by the external gate voltage applied across a dielectric layer. In this case, the connection of the electric field with the localized magnetic states occurs via the exchange interaction of polarized itinerant electrons with the localized magnetic states. The corresponding mechanism of the magnetic anisotropy formation and its dependence on the interface electron structure are described in the framework of a tight-binding model of spin-orbit-coupled electrons exchange-coupled to the localized magnetic states.

Acknowledgements

This work is part of a project that has received funding from the European Union's Horizon 2020 research and innovation programme under the Marie Skłodowska-Curie grant agreement No 778308.

References

[1] A. Kirilyuk, A. V. Kimel, and T. Rasing, "Laser-induced magnetization dynamics and reversal in ferrimagnetic alloys," Rep. Prog. Phys., vol. 76, 026501, May 2013.

[2] A. Hofmann, Y. Tserkovnyak, G. S. D. Beach, E. E. Fullert, C. Leighton, A. H. MacDonald, D. C. Ralph, D. A. Arena, H. A. Dürr, K. P. Fischer, J. Groller, J. P. H. Heremans, T. Jungwirth, "Interface-induced phenomena in magnetism," Rev. Mod. Phys., vol. 89, 025006, June 2017.

[3] R. Hertel, "For faster magnetic switching− destroy and rebuild," Physics. vol. 2, 73, September 2009.

[4] K. Vahaplar, A. M. Kalashnikova, A. V. Kimel, D. Hinzke, U. Nowak, R. Chantrell, A. Tsukamoto, A. Itoh, A. Kirilyuk, T. Rasing, "Ultrafast Path for Optical Magnetization Reversal via a Strongly Nonequilibrium State," Phys. Rev. Lett., vol. 103, 117201, September 2009.

[5] R. F. L. Evans, D. Hinzke, U. Atxitia, U. Nowak, R. W. Chantrell, O. Chubykalo-Fesenko,'Stochastic form of the Landau-Lifshitz-Bloch equation,' Phys. Rev. B. 85, 014433, January 2012.

[6] R. F. L. Evans, U. Atxitia, and R. W. Chantrell, "Quantitative simulation of temperature-dependent magnetization dynamics and equilibrium properties of elemental ferromagnets," Phys. Rev. B 91, 144425, April 2015.

[7] I. Radu, K. Vahaplar, C. Stamm, T. Kachel, N. Pontius, H. A. Dürr, T. A. Ostler, J. Barker, R. F. L. Evans, R. W. Chantrell, A. Tsukamoto, A. Itoh, A. Kirilyuk, Th. Rasing, A. V. Kimel, "Transient ferromagnetic-like state mediating ultrafast reversal of antiferromagnetically coupled spins," Nature, vol. 472, 205, April 2011.

[8] R. Cheng, J.-G. Zhu, D. Xiao, "Dynamic Feedback in Ferromagnet Spin Hall Metal Heterostructures," Phys Rev. Lett., vol. 117, 097202, August 2016.

[9] S. E. Barnes, J. Ieda, S. Maekawa,"Rashba Spin-Orbit Anisotropy and the Electric Field Control of Magnetism,"Sci. Rep., N 4, 1, February 2014.

[10] E. I. Dzyaloshinksky, Thermodynamic theory of "weak" ferromagne-tism of antiferromagnetics," J. Phys. Chem. Solids, 4, 241, January (1958).

[11] T. Moriya,"Anisotropic superexchange interaction and weak ferro-magnetism," Phys. Rev. Lett., 120, 91, October 1960.

[12] A. Manchon, H. C. Koo, J. Nitta, S. M. Frolov, and R. A. Duine,"New perspectives for Rashba spin - orbit coupling," Nat. Mater. 14, 871 February 2015.

[13] D. Chiba D., M. Sawicki, Y. Nishitani, Y. Nakatani, F. Matsukura, and H. Ohno, "Magnetization vector manipulationby electric fields," Nature 455, 515, August 2008.

[14] T Maruyama, Y Shiota, T Nozaki, K Ohta, N Toda, M Mizuguchi, AA Tulapurkar, T Shinjo, M Shiraishi, S Mizukami, et al., "Large voltage-induced magneticanisotropy change in a few atomic layers of iron," Nat. Nanotechnol. 4, 158, December 2009.

[15] G. Chaudhary, M. S. Dias, A. H. MacDonald, S. Lounis, "Anatomy of magnetic anisotropy induced by Rashba spin-orbit interaction," Phys. Rev. B 98, 134404, October 2018.